VOL. 8, NO. 7, JULY 2013 ISSN 1819-6608
ARPN Journal of Engineering and Applied Sciences


www.arpnjournals.com

CFD SIMULATION OF A SINGLE PHASE FLOW IN A PIPE SEPARATOR USING REYNOLDS STRESS METHOD

Eyitayo A. Afolabi[1] and J. G. M. Lee[2]
[1]Department of Chemical Engineering, Federal University of Technology, Minna, Nigeria
[2]School of Chemical Engineering and Advanced Materials, Newcastle University, Newcastle upon Tyne, UK
E-Mail: elizamos2001@yahoo.com

ABSTRACT

The Reynolds stress method of commercial ANSYS FLUENT software is used for the numerical simulation of the single phase flow in a 30mm ID pipe separator. The CFD predicted results is then compared with the stereoscopic PIV measurements at the three different axial positions. The comparison between the experimental and computational results showed good qualitative agreement at most axial positions within the pipe separator and considerable insight was gained into the flow mechanism. However, there were some discrepancies between the CFD results and the SPIV measurements at some axial positions away from the inlet section. Therefore, Reynolds stress model (RSM) is deemed to be a good methodology for modelling the hydrodynamic behaviour in a pipe separator system.

Keywords: numerical simulation, pipe separator, Reynolds stress model, velocity distribution.

1. INTRODUCTION

Separators are devices widely used in the industrial and manufacturing sector to separate disperse phase from continuous phases in accordance to density and particle size. The popularity of pipe separator is due to fact that it is simple to construct, do not require extensive cost and maintenance, and show relatively high separation efficiency. Three phase pipe separator is an extension of the Gas-Liquid and Liquid-Liquid cylindrical cyclone technologies developed to separate gas-liquid-liquid mixtures by the University of Tulsa, USA (Vazquez, 2001). The complex flow phenomenon involved in cyclones coupled with the non-availability of high speed computational systems has until recently restricted most research work to focusing on empirical modelling. These empirical models are developed from analysis of the experimental data such as the effects of operational and geometrical variables. The four basic parameters used to specify the performance of a cyclone are the particle size which corresponds to the proportion of overflow to underflow, the flow split between the overflow and underflow, the pressure drop and the sharpness of separation (Pericleous and Rhodes, 1986).

In recent years, however the emergence of more powerful computers with large storage and high capacity processing facilities has provided the basis whereby computational fluid dynamics (CFD) can be used to predict flow pattern velocity profiles under a wide range of design and operating conditions. This has led to a better understanding of the turbulent flow behaviour in cyclones (Tu *et al*., 2008; Wilcox, 1993).

Several features of cyclone or pipe separators modelling such as knowledge of the flow structure, the nature of air-core development, fluid- fluid and fluid-wall interactions are essential in providing the opportunity for design modifications to achieve improved separation. The following features make turbulence inside the cyclone separator highly anisotropic:

a) High curvature of the average streamlines: This leads to the developments of secondary flows which continue to evolve due to the cylindrical geometry (He *et al*., 1999).
b) High swirl intensity and radial shear: As a result of the tangential inlet, high swirl flow develops with shear stress as the fluid moves along the solid boundary.
c) Adverse pressure gradients and recirculation zones. When any of the outlets are open to the atmosphere, there is a negative pressure difference at the centre of the tube, and this result in the formation of an air core along the cyclone axis (Cullivan *et al*., 2004).

Advances in numerical modelling techniques and computers, have provided engineers with a wide selection of commercially available fluid flow models based on the Navier-Stokes equations. Most commercial CFD package offers Reynolds Averaged Navier Stoke (RANS) models such as, the k-ε model, the renormalization group model, the anisotropic Reynolds stress model, and the large eddy simulation (LES) turbulence model. The fluctuating motion in the presence of swirl intensity is found to be anisotropic and this invalidates some of the assumptions upon which simple turbulence models are based. Therefore, mixing-length and the standard k-ε models are insufficient for computing strong swirling flows in cyclones (Cullivan *et al*., 2003; Suasnabar, 2000; Slack and Wraith, 1997). In order to solve this problem, the renormalization group (RNG) k-ε model was developed with a correction for swirl and showed significant improvement for modelling fairly rotational flow (Pericleous, 1987). Earlier discussion of the numerical simulation advocated that RSM gives the best approximation of the measured velocity profiles and is a good indication of its suitability to model the anisotropic turbulence feature in a cyclone. However, RSM simulation can be inherently unstable and slow. It is therefore better to obtain a solution using the k-ε model before activating the RSM calculation. The LES approach seems to offer a

good alternative to classical turbulence models when applied to the numerical solution of fluid flows within the cyclones. However, because of the high number of grids required and the complexity of today's industrial cyclone separator simulations, the unsteady Reynolds Averaged Navier Stoke (RANS) approach with higher order turbulence closure is a better option that gives affordable and realistic predictions of flow fields inside cyclones (Utikar *et al*., 2010; Delgadillo and Rajamani, 2007; Versteeg and Malalasekera, 2007; Slack *et al*., 2004).

In this paper, a CFD package ANSYS FLUENT is used to simulate the single unsteady water flow in a 30mm ID pipe separator and the 3-D numerical solution results are then compared with the experimental measurements using the Stereoscopic Particle Image Velocimetry technique. By comparing the predicted velocity profile against those measured data, the numerical model's ability to describe the flow patterns that occur in the real flow system could be determined, and subsequently validated for use in the optimization study.

2. MODEL EQUATIONS

The separation process in cyclone occurs in an extremely short residence time such that there is no opportunity for significant heat exchange with the surroundings (Almgren *et al*., 2006). Therefore, a flow in pipe separator is with low dissipation (indicated by low pressured drop) and hence little internal heating. For an incompressible, isothermal Newtonian flow (ρ = constant, μ = constant), with a velocity field $\vec{V} = (u_r, u_\theta, u_z)$, only the mass and momentum balance equations need to be considered.

2.1. Reynolds average navier stokes equations

The continuity and momentum equations for an incompressible fluid can be written as:

$$\frac{\partial \rho}{\partial t} + \frac{\partial}{\partial r_i}(\rho u_i) = 0 \quad (1)$$

$$\frac{\partial}{\partial r_i}(\rho u_i u_j) = -\frac{\partial p}{\partial r_i} + \frac{\partial}{\partial r_j}\left[\mu\left(\frac{\partial u_i}{\partial r_j} + \frac{\partial u_j}{\partial r_i} - \frac{2}{3}\delta_{ij}\frac{\partial u_i}{\partial r_i} + \frac{\partial}{\partial r_j}\right) - \rho\overline{u'_i u'_j}\right] \quad (2)$$

Equations (1) and (2) are referred to as Reynolds-averaged Navier-Stokes (RANS) equations. The presence of the Reynolds stress term $-\rho\overline{u'_i u'_j}$ in equation (2) means that there is need to introduce additional terms in the governing equations. The two main approaches used to solve the Reynolds stress terms that appear as unknowns in the RANS equations are, firstly, to find an expression to represent the Reynolds stress (Eddy viscosity modelling). Secondly, to use additional equations such as differential transport equations for Reynolds stress in second moment closure modelling (Tu *et al*., 2008; Versteeg and Malalasekera, 2007; Pope, 2000).

2.2. Reynolds stress model

The Reynolds stress model (RSM) adopts an approach whereby the model transport equations are solved for the individual Reynolds stresses and for the dissipation rate so as to close the Reynolds-averaged Navier Stokes equations. The exact Reynolds stress transport equation accounts for the directional effects of the Reynolds stress fields.

The transport equations for the Reynolds stresses may be written as follows:

$$\tau_{ij} = \overline{\rho u'_i u'_j} \quad (3)$$

$$\frac{\partial \rho \overline{u_i u_j}}{\partial t} + \frac{\partial}{\partial r_k}\left(\rho u'_k \overline{u'_i u'_j}\right) = P_{ij} + F_{ij} + D_{Tij} + \phi_{ij} - \varepsilon_{ij} \quad (4)$$

$$P_{ij} \text{ (stress production)} = -\left(\overline{u'_i u'_k}\frac{\partial u_j}{\partial r_k} + \overline{u'_j u'_k}\frac{\partial u_i}{\partial r_k}\right) \quad (5)$$

$$F_{ij} \text{ (rotation production)} = -2\rho\Omega_k\left(\overline{u'_j u_m}\,\varepsilon_{ikm} + \overline{u'_i u_m}\,\varepsilon_{jkm}\right) \quad (6)$$

$$D_{Tij} \text{ (turbulent diffusion)} = -\frac{\partial}{\partial x_k}\left(\rho\overline{u'_i u_j u_k} + \left(\overline{\rho(\delta_{kj}u'_i - \delta_{ik}u'_j)}\right)\right) \quad (7)$$

$$\phi_{ij} \text{ (pressure strain)} = \left(\overline{\frac{\partial u'_i}{\partial r_j}} + \frac{\partial u_j}{\partial r_i}\right) \quad (8)$$

$$\varepsilon_{ij} \text{ (dissipation)} = -2\mu\,\overline{\frac{\partial u'_i}{\partial r_k}\frac{\partial u_j}{\partial r_k}} \quad (9)$$

In order to mathematically close equation (4), approximations are made for the diffusion, dissipation rate and pressure strain terms. Further information on the under-lying equations for the Reynolds stress method can be found in Versteeg and Malalasekera, (2007) Pope, (2000) and Launder and Spalding, (1974).

3. NUMERICAL STUDY

3.1. Model geometry and mesh

The geometry of the pipe separator used in the CFD simulation is shown in Figure-1, and was used for the

experimental investigation of multiphase flow using Stereoscopic Particle Image Velocimetry technique (Afolabi, 2012). The pipe separator was a transparent cylinder with a vertical section measured 1675 mm by height and inside diameter of 30 mm. The tangential inlet, inclined at an angle of 27 degrees, was designed in such a way that it dimensions gradually reduce to 25% of the cross-sectional area and attached to the vertical cylinder 585 mm from the top. The diameter of the overflow, water-rich and oil-rich underflow tubes are 20 mm, 20 mm and 10 mm, respectively. The water rich outlet was located at right angles to the cyclone 185 mm above the base, while the overflow and oil rich outlets were located at the top and bottom of the cyclone, respectively. This geometry corresponds to a numerical solution domain with dimension of 0.885m, 1.820m and 0.646m in radial, axial and tangential direction, respectively and then subdivided into discrete volume through computational grid in space.

Hexahedral and tetrahedral meshing schemes of a commercial pre-processor, GAMBIT from Fluent Inc. were used to mesh the model geometry. The section where the tangential inlet joins the main cyclone body and the point where the water rich outlet joins the main body were both meshed using a tetrahedral mesh type. This mesh type was used because it can be easily adjusted to suit the complex geometry. An unstructured hexahedral mesh type was selected to mesh the rest of the separator, as it was found to align easily with flow direction, thereby reducing numerical diffusion when compared with other mesh types such as the tetrahedral (Slack *et al*., 2004). The three outlets as shown in Figure-1 were all defined as outflows and this was based on the assumption that the diffusion fluxes in the direction normal to the outlet are zero. The tangential inlet was prescribed as a velocity inlet and the rest of the body surfaces (with the exception of the three outlet faces) were treated as solid walls with no slip boundary condition applied. That is, all the three velocity components were zero at the wall.

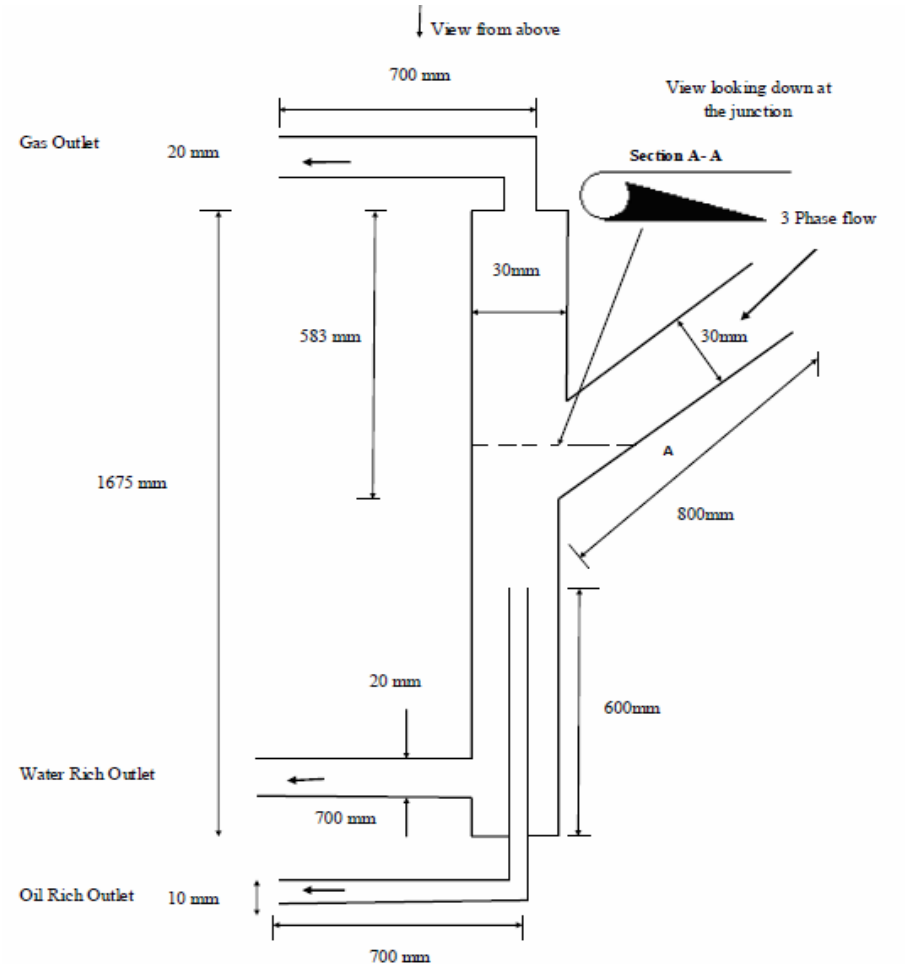

Figure-1. Schematic of pipe separator.

3.2. Numerical simulation

The grid independence study was conducted with five different grid sizes with cell counts varying from 50, 000 to 300, 000. It was observed that the numerical results obtained became independent of the total number of computational cells beyond 225, 000. In the rest of this

work, the total number of computational cells used to discretize the entire geometry was 225, 000. This was found optimal for good predictions using RSM and in consideration of the computational time required.

A segregated, 3-D double precision implicit solver was used for the CFD simulation of the single flow of water inside the 30 mm ID pipe separator and the Semi-Implicit Method for Pressure Linked Equations (SIMPLE) algorithm used for solving the continuity and momentum equations. In order to correctly predict the characteristic of the prevailing highly swirling flow within the pipe separator, the Pressure Staggered Option (PRESTO) was adopted for the pressure interpolation scheme in order to discretize the pressure gradient term (Versteeg and Malalasekera, 2007). The standard wall function (Launder and Spalding, 1974) was used for the near-wall treatments of the wall boundaries. Operating conditions were specified as being standard atmospheric pressure (101325 Pa) with gravitational acceleration taken as 9.81 $m/s^2$and defined to act downwards in the main body of the pipe separator.

A water flow rate of 0.000196 m^3/s was set at the inlet with the turbulent intensity of 4.8%. In this study, water flowed out of the outlet such that the percentage of water as a fraction of the inlet mass flow was 60% through the air outlet, 33% through the water-rich outlet and the balance through the oil-rich outlet. It was reported that higher order discretization schemes provide better accuracy than first and second order schemes for grids aligned with the flow direction, especially for rotating and swirling flows (Slack, 2004). However, for the initial simulation, the default first order scheme was used to discretize the momentum, turbulent kinetic energy, dissipitation rate and Reynolds stress terms. Then, after it converged, the second-order scheme and Quadratic Upwind Interpolation for Convective Kinetic (QUICK) were subsequently activated.

The two basis assumptions used in this study are:

a) The boundary condition for the inflow velocity at the pipe separator inlet was assumed to be uniform.
b) No slip boundary condition for which all three components of velocity are identically zero at the wall was used for all numerical simulations in this study.

The water flow field was pre-established through the steady state simulation using the standard k-ε model with a convergence criterion of at least 10^{-4}. The residuals exhibited a cyclic pattern, indicating the inadequacy of the steady state solver. In order overcome this problem, the transient solver with time step of 0.001 seconds was subsequently activated. Therefore, the single phase water flow in the pipe separator was treated as the unsteady, isothermal flow of a viscous, incompressible fluid. Since the flow field in the pipe separator was found to be highly swirling and anisotropic in nature, the converged k-ε model solution is then switched to Reynolds Stress Model (RSM). In order to ensure that the flow features were fully developed, the transient simulation was run for at least 12 seconds (more than mean residence time of 10 seconds).

4. RESULTS AND DISCUSSIONS

Figures 2 to 4 show the comparison of the numerical simulation of the water flow fields with the stereoscopic.

PIV measurements at the three different axial positions of Z = -395mm, -75mm and 295mm as illustrated in Figure-1.

4.1. Tangential velocity

Figure-2 (a - c) compare the CFD simulation results with the measured mean tangential velocity profiles at the axial positions of Z=- 0.395 m, - 0.750 m and 0.295 m respectively. The trend exhibited by the CFD predicted tangential velocity profiles at all axial positions consist of two regions which are similar to those obtained using SPIV measurements. Firstly, there is an outer free vortex region often referred to as free vortex where the tangential velocity decreases with increasing distance from the centre of the tube. Secondly, a forced vortex at the centre where tangential velocity increases with radius. Studies of the tangential velocity with similar qualitative behaviour have also been done by Bergstrom and Vomhoff (2007), Dlamini *et al*., (2005) and Slack *et al*., (2004).

The tangential velocity profile is observed to be over-predicted in the CFD simulation at Z = -0.395 m and under-predicted at the Z = -0.750 m axial position. At Z = 0.295 m, the tangential velocity profile is observed to be under-predicted moving away from the centre of the tube and over-predicted at the wall. For example, Figure-2(a) showed that the maximum tangential velocities from the experimental data are 0.175 m/s at x = − 7.5 mm and 0.225 m/s at x = 11 mm. However, the maximum tangential velocities in the simulation results are 0.25 m/s at x = − 4 mm and 0.275 m/s at x = 9.5 mm. In Figure-2(b) the best agreement occurs at x = ± 7.5 mm, where the prediction is within 2% of the experimental profile for the majority of the x-axis coordinates. As we approach the wall region, the predicted tangential velocity profile is found to be under-predicted by 5% and 12% near to the wall at the negative and positive values of the x-axis, respectively. The simulated profile in Figure-2(c) shows that the CFD package is able to capture the lowest velocity profiles at the centre of the tube which are absent in the experimentally determined profile. This is due to high swirl that displace tracer particles away from the centre of the tube, thereby reducing the amount of tracer particles to be illuminated and recorded during SPIV measurement. It was observed that the free vortex region starts at smaller values of the radius (Figure-2a) and larger values of the radius (Figures 2b and c) for the CFD simulation in comparison with the experimental data.

The CFD results confirmed that the tangential velocity component is the main velocity component that affects the swirling flow field and its interaction with strong shear in the radial direction produces centrifugal forces that determine particle separation. An increasing

tangential velocity profile towards the centre supports the assumption of the free vortex flow typical of the anisotropic turbulent flow field in the pipe separator. This means, flow shear is present in the free vortex region and thereby promotes particle dispersion (Slack, 1997).

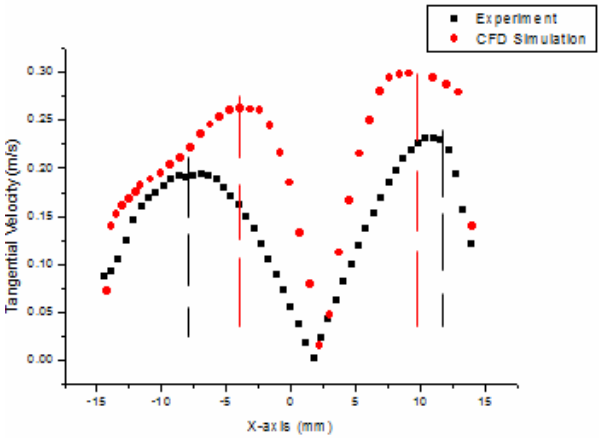

(a)

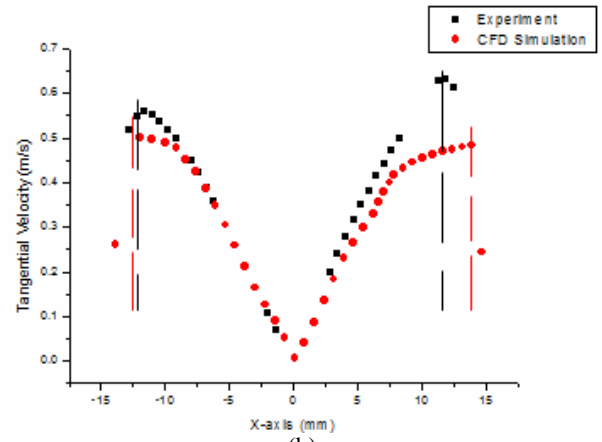

(b)

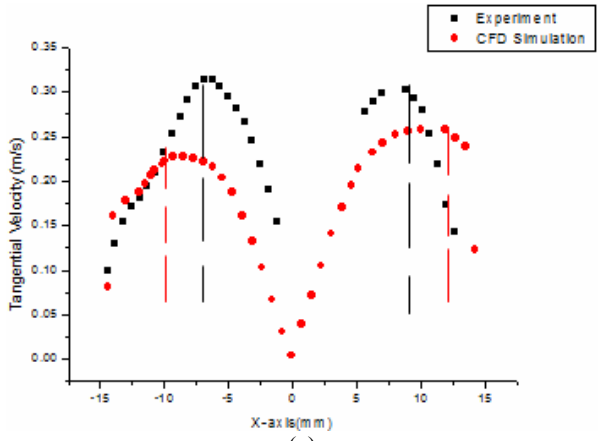

(c)

Figure-2. Comparison of the CFD result and experimental data for mean tangential velocity at axial positions of (a) Z = -0.395m (b) -0.750m (c) 0.295m.

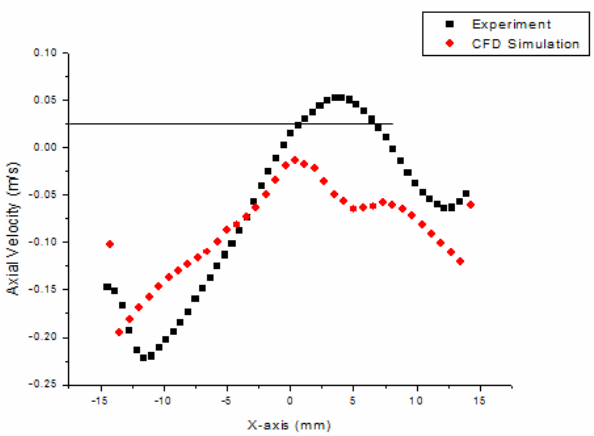

(a)

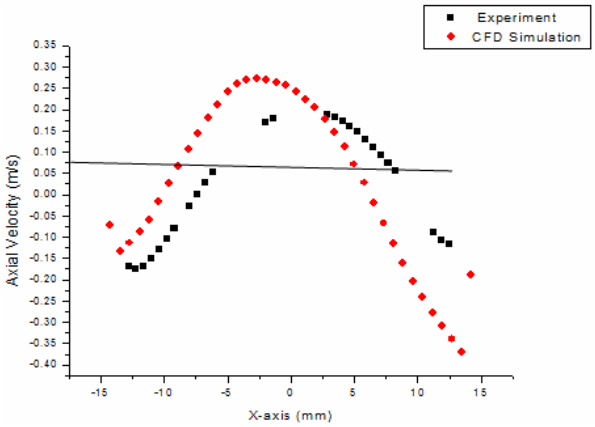

(b)

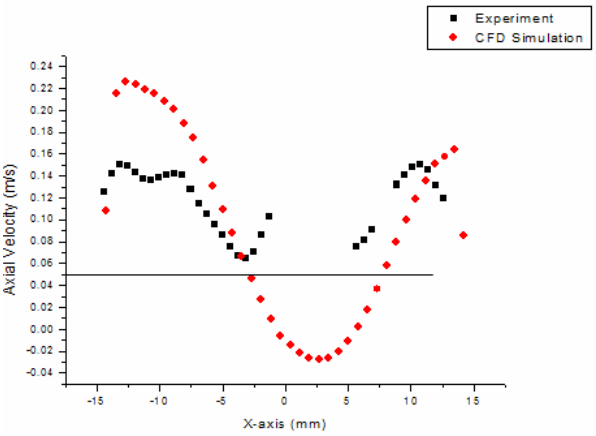

(c)

Figure-3. Comparison of the CFD result and experimental data for mean Axial Velocity at Axial Positions of (a) Z = -0.395 m (b) -0.750 m (c) 0.295 m.

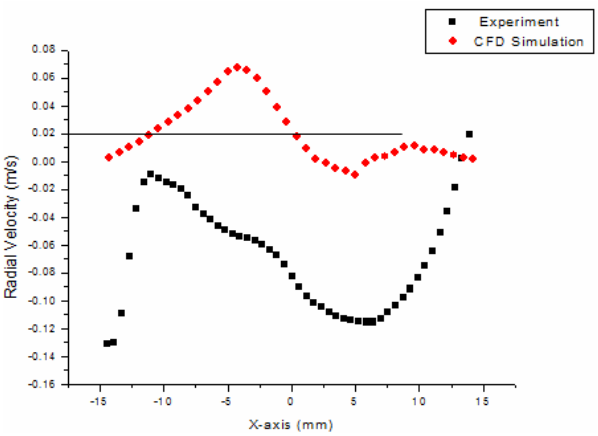

(a)

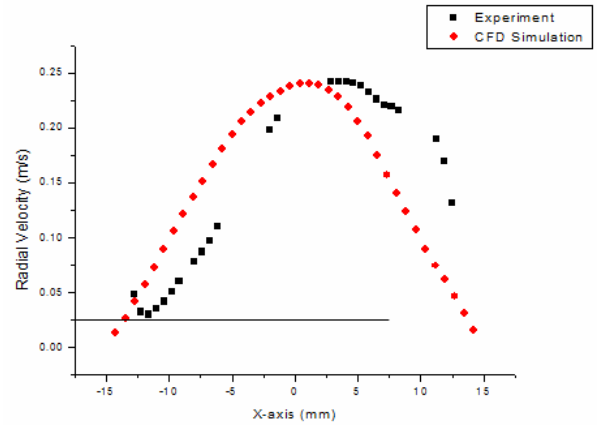

(b)

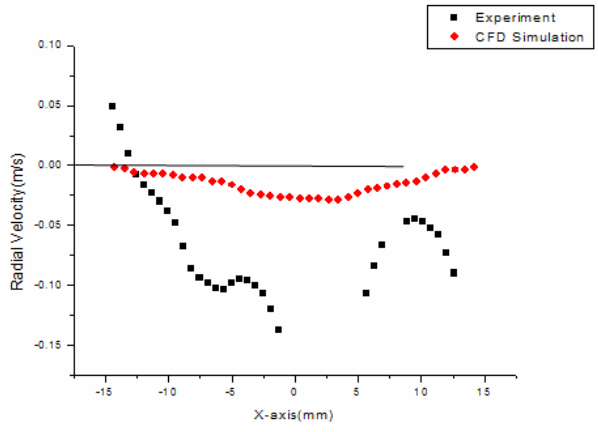

(c)

Figure-4. Comparison of the CFD result and experimental data for mean radial velocity at axial positions of (a) Z = -0.395 m (b) -0.750 m (c) 0.295 m.

4.2. Axial velocity

Figure-3 presents a comparison of the mean axial velocity profiles obtained by the CFD simulation and the SPIV measurements. The computational model gives qualitative agreement with the experimental measurements at Z = −0.750 m position and disagreement at Z=−0.395 m and 0.295 m especially at the centre of the tube. For example, at Z = − 0.395 m the measured profile indicated the presence of an upward flow at the centre of the tube but absent in the predicted profile. In addition, the predicted profile in Figure-3(c) showed the presence of a downward flow at the centre of the tube, however, there is no experimental data at the centre of the tube to validate the predicted result. This discrepancy is probably due to slippage of the tracer particle caused by large acceleration at the centre of the tube. As a result, there is no particle to scatter light to be recorded with SPIV system.

4.3. Radial velocity

Figure-4 shows the comparison of the mean radial velocity distributions at the three axial positions as measured experimentally and simulated using CFD. The CFD flow pattern at Z = − 0.75 m and 0.295 m compare favourably with experimental data except at few x-axis coordinates where measured profile shows an outward flow pattern. However, there is disagreement between the flow patterns as measured and predicted at axial position of Z = − 0.395 m. The value of the predicted radial velocity in Figure-4(b) is larger at negative values of the x-axis and smaller at positive values of the x-axis in comparison with the measured radial velocity. For example, the measured radial velocity at x= 7.5mm is 0.21m/s, whereas the predicted radial velocity is 0.15m/s.

5. CONCLUSIONS

A comparison of the experimental and computational results showed that good qualitative agreement was obtained at most axial positions, but the magnitude of the velocity profiles was not predicted correctly. The tangential velocity profiles predicted by the CFD simulation are similar to those of the experimental data. Far away from the inlet region, the CFD model was found to predict different axial and radial velocity profiles at the centre of the tube. We can then conclude that the numerical CFD simulation using ANSYS FLUENT can predict the flow pattern quantitatively correctly and can provide an alternative method for studying fluid dynamics inside pipe separators and improve performance parameters.

ACKNOWLEDGEMENT

This research has been supported by the PTDF, Nigeria.

Nomenclature

C_1	Constant (RSM pressure strain correlation term) (dimensionless)
C_2	Constant (RSM pressure strain correlation term) (dimensionless)
D_{ij}	Diffusion term (RSM) (m^2/s)
F_{ij}	Rotation production (RSM) (m^2/s)
k	Turbulent kinetic energy (m^2/s^2)

p Pressure (N/m^2)
P_{ij} Production term of RSM (m^2/s)
ρ Density (kg/m^3)
u, v, w Fluctuating components in the r, θ , z directions (m/s)
i, j, k Computational coordinates system
r, θ ,z Cylindrical coordinates
ε Dissipation of turbulent kinetic energy (m^2/s^3)
ε_{ij} Rate of dissipation of Reynolds stress (kg/m^3s)
μ Dynamic viscosity (kg/ms)
μ_t Turbulent dynamic viscosity (kg/ms)
τ Shear stress (Pa)
τ_{ij} Surface stress tensor (Pa)
$\tau_{ij,\varepsilon}$ Reynolds stress tensor (Pa)
ν *v* Kinematic viscosity (m^2/s)
υ_t Kinematic turbulent viscosity (m^2/s)
δ Delta function (dimensionless)
ϕ_{ij} Pressure strain

REFERENCES

Afolabi E.A. 2012. Experimental Investigation and CFD Simulation of Multiphase flow in a Three Phase Pipe Separator. Unpublished Ph.D Thesis. Newcastle University, Newcastle, UK.

Almgren A.S., Bell J.B., Rendleman C.A. and Zingale M. 2006. Low Mach number Modelling of Type Ia Supernovae. I. Hydrodynamics. Astrophysical Journal. 637(2): 922-936.

Bergström J. and Vomhoff H. 2007. Experimental hydrocyclone flow field studies. Separation and Purification Technology. 53(1): 8-20.

Cullivan J. C., Williams R. A., Dyakowski T. and Cross C. R. 2004. New understanding of a hydrocyclone flow field and separation mechanism from computational fluid dynamics. Minerals Engineering. 17(5): 651-660.

Cullivan J. C., Williams R. A. and Cross C. R. 2003. New insights into hydrocyclone operation. Particulate Science and Technology. 21(1): 83-103.

Delgadillo J. A. and Rajamani R. K. 2007. Exploration of hydrocyclone designs using computational fluid dynamics. International Journal of Mineral Processing. 84(1-4): 252-261.

Dlamini M. F., Powell M. S. and Meyer C. J. 2005. A CFD simulation of a single phase hydrocyclone flow field. Journal of the South African Institute of Mining and Metallurgy. 105(10): 711-717.

He P., Salcudean M. and Gartshore I. S. 1999. A numerical simulation of hydrocyclones. Chemical Engineering Research and Design. 77(A5): 429-441.

Launder B. E. and Spalding D. B. 1974. The numerical computation of turbulent flows. Computer Methods in Applied Mechanics and Engineering. 3(2): 269-289.

Pericleous K. A. 1987. Mathematical simulation of hydrocyclones. Applied Mathematical Modelling. 11(4): 242-255.

Pericleous K. A. and Rhodes N. 1986. The hydrocyclone classifier - A numerical approach. International Journal of Mineral Processing. 17(1-2): 23-43.

Pope S. B. 2000. Turbulent flows. Cambridge; New York: Cambridge University Press.

Slack M. D., Del Porte S. and Engelman M. S. 2004. Designing automated computational fluid dynamics modelling tools for hydrocyclone design. Minerals Engineering. 17(5): 705-711.

Slack M. D. and Wraith A. E. 1997. Modelling the velocity distribution in a hydrocyclone. 4th International Colloquium on Process Simulation, 11-13 June, Espoo Finland. pp. 65-83.

Slack M. D. 1997. Separation of particles from liquids by the solid core cyclone. Thesis. Newcastle University, UK.

Suasnabar D. 2000. Dense Medium Cyclone Performance, Enhancements via Computational modeling of the physical process. Thesis. University of New South Wales.

Tu J., Yeoh G.H, and Liu C. 2008. Computational Fluid Dynamics: A Practical Approach. 1st edition, Elsevier Inc. Oxford, UK.

Utikar R., Darmawan H., Tade M., Li Q., Evans G., Glenny M. and Pareek V. 2010. Hydrodynamic Simulation of Cyclone Separators. Computational Fluid Dynamics. Hyoung Woo OH (Ed.). ISBN 978-953-7619-59-6, www.intechopen.com.

Vazquez C. O. 2001. Multiphase flow separation in Liquid-Liquid cylindrical cyclone and Gas-Liquid -Liquid cylindrical cyclone compact separators. Thesis. The University of Tulsa, U.S.

Versteeg H. K. and Malalalsekera W. 2007. An introduction to computational fluid dynamics: the finite volume method Harlow Prentice Hall.

Wilcox D. C. 1993. Turbulence modeling for CFD'. La Canada, DCW Industries Inc.